J. Fluid Mech. (2015), *vol.* 779, *pp.* 842–858.
doi:10.1017/jfm.2015.463

Analysis of the pressure buildup behind rigid porous media impinged by shock waves in time and frequency domains

O. Ram[1] **and O. Sadot**[1,†]

[1]Pearlstone Center for Aeronautical Engineering Studies, Protective Technologies R&D Center, Department of Mechanical Engineering, Faculty of Engineering Sciences, Ben-Gurion University of the Negev, Beer Sheva 8410501, Israel

(Received 24 November 2014; revised 17 May 2015; accepted 3 August 2015; first published online 26 August 2015)

The transformation of a time-dependent pressure pulse imposed on the front face of a rigid porous medium sample, mounted in a tunnel, through the sample and a fixed-volume air gap between the rear face of the sample and the end wall of a tunnel is studied both experimentally and analytically. In the experiments, rigid porous samples that are placed at various distances from a shock tube end wall are subjected to the impingement of shock waves. The pressure buildup behind the porous sample is monitored and compared with the pressure imposed at the front face of the porous sample. The shock tube is fitted with a short driver section in order to generate blast-like decaying pressure profiles, which continue to decay after the initial shock impingement. In this scenario, the measured pressure profile at the end wall, which is affected by the properties of the porous medium and the size of the air gap separating its rear face and the shock tube end wall, is significantly different from the pressure profile imposed on the front face of the porous sample. The mechanism governing the pressure transformation provided by the porous medium is attributed to a selective filtration process that attenuates the pressure changes associated with high frequencies. The results of the present study are also analysed in conjunction with previously published analytical and numerical models to achieve a broader understanding of the physical mechanisms affecting the pressure buildup.

Key words: compressible flows, shock waves

1. Introduction

Porous foams can be divided into aqueous foams (Panczak, Krier & Butler 1987; Larsen 1992; Ball & East 1999; Britan *et al.* 2012, 2013), flexible foams (Skews 1991; Ben-Dor *et al.* 1992, 1994, 1996*a*,*b*; Olim *et al.* 1994; Kitagawa, Yasuhara & Takayama 2006; Seitz & Skews 2006) and rigid foams (Levy *et al.* 1993; Kazemi-Kamyab, Subramaniam & Andreopoulos 2011; Ram & Sadot 2013). These studies emphasized the importance of the qualitative description of the shock–structure interactions, the resultant flow field and the stress reduction or amplification due to

† Email address for correspondence: sorens@bgu.ac.il

the presence of porous barriers. They also revealed that the physics involved in the shock impingement on a porous medium is very complicated, and, as a result, very sophisticated modelling and numerical analysis are required to analyse the related phenomena.

It is well known that obstacles placed in the path of a moving shock can cause significant diffraction and attenuate the shock wave transmitted through them (Onodera 1998). The use of barriers as a means of mitigating blast waves has been suggested by many investigators (Ohtomo, Ohtani & Takayama 2005; Britan *et al.* 2006; Kitagawa *et al.* 2006; Seeraj & Skews 2009; Berger, Sadot & Ben-Dor 2010, 2012; Igra *et al.* 2012). These studies indicated that the main parameter affecting the shock wave attenuation is the blockage ratio facilitated by the barriers. The shape of the barrier, the resistance to the flow passing through the barrier and the geometrical material properties were found to also contribute to the shock wave attenuation. An important application of shock wave attenuation is protection against blast waves in explosion scenarios in mine tunnels, transportation tunnels, various tubes and vents, etc. These scenarios pose an even greater difficulty due to channelling and confinement effects (van den Berg & Weerheijm 2006; Silvestrini, Genova & Leon Trujillo 2009; Benselama *et al.* 2010; Langdon, Nurick & du Plessis 2011). An important particular problem emerges when a target is protected by porous barriers, which span across the entire cross-section of a tunnel leading to the target. This scenario can be encountered, for example, in shelter vents leading to fragile ventilation filters and in tunnels leading to the blast doors of bunker entrances. In these scenarios, in the absence of means of protection, the incident shock wave is reflected head-on at the end of the tunnel and the load imposed on it could be destructive. In this context, several researchers have suggested the use of porous foams as a barrier to mitigate the load imposed on the end of the tunnel. Study of the flow field developed during the interaction of shock waves with porous media falls under the broader spectrum of shock-wave–structure interaction studies. These have many applications such as in chemical manufacturing processes, mufflers, supersonic flight and more.

The present study presents a new approach for analysing the flow field that results from the impingement of a shock wave on a rigid porous medium. In this approach, two modelling techniques (numerical and empirical), which have been previously presented, are employed in conjunction to facilitate a new and a better understanding of the important physical mechanisms involved.

1.1. *Shock interaction with a rigid porous medium*

Skews, Atkins & Seitz (1992), Levy *et al.* (1993), Levy, Ben-Dor & Sorek (1996, 1998), Andreopoulos, Xanthos & Subramaniam (2007) and Kazemi-Kamyab *et al.* (2011) have conducted several studies on the interaction of shock waves with rigid porous media in which the skeleton of the porous medium remained incompressible when impinged by the shock waves. In these studies, the filtration effect was well documented to be the governing mechanism affecting the shock wave passage through the porous medium and the development of the flow field inside and in the vicinity of the porous medium. In these investigations, rigid porous samples were placed either adjacent to a shock tube end wall or with a predetermined air gap, i.e. standoff distance (SOD), between the rear face of the porous sample and the shock tube end wall. The investigations revealed that the pressure that was developed on the end wall was affected by the shock wave strength, the fluid properties, the porous sample properties and the standoff distance, which determines the volume of the abovementioned air gap (Levy *et al.* 1993).

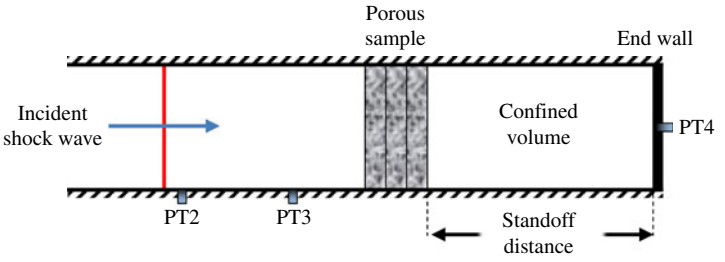

FIGURE 1. (Colour online) A schematic illustration of the investigated problem: a shock or blast wave impinges on the front face of a sample made of an open-cell rigid porous material that protects the end wall of a tunnel. A volume is confined between the rear face of the porous sample and the end wall. PT2 and PT3 are pressure transducers flush mounted on the side wall. PT4 is a pressure transducer mounted on the end wall.

In more recent research, Kazemi-Kamyab *et al.* (2011) studied experimentally the stress transmitted to the end wall of a shock tube shielded by a rigid porous medium. They showed that the introduction of a fixed air gap between the porous sample and the end wall decreased the stress transmitted to the end wall. In this case, the propagation of the waves ahead of, inside and behind the porous sample is more complicated. They showed that the pressure behind the sample rose gradually as expected and reached asymptotically the same value as that at the front face of the sample. They noted that a shock wave transmitted through the porous sample reverberated in the gap between the rear face of the porous sample and the end wall. Kazemi-Kamyab *et al.* (2011) found that the stress transmitted to the end wall of the shock tube was a function of the geometrical material properties and the size of the air gap.

1.2. *The investigated problem*

As described, a rigid porous sample significantly increases the pressure buildup time at the tunnel end by inhibiting the flow into the confined volume behind the porous sample. These effects are significantly amplified when a gap is introduced between the rear face of the porous sample and the end wall. The porous medium effects can be simply characterized by the change of the pressure profile from the input step function profile that is imposed by the impinging shock wave on the front face of the porous sample to the output profile that is obtained at the end wall behind the air gap. This difference is a direct consequence of the flow passage through the porous sample and the confined volume in the gap between the rear face of the porous sample and the end wall. The influence of the various governing parameters in this problem requires further elaborations which in turn could lead to better design methodologies. A schematic illustration of the investigated problem is presented in figure 1.

The governing parameters of the problems are as follows.

(i) The input pressure profile imposed on the front face of the porous sample by the shock or the blast wave, $P_{in}(t)$.

(ii) The volume between the rear face of the porous sample and the end wall. The volume is determined by the standoff distance, SOD, between the rear face of the porous sample and the end wall.

(iii) The effective length of the porous sample, $L_{eff} = \phi L$, where L is the length of the porous sample and ϕ is the porosity, i.e. the volume of air inside the porous medium divided by the volume of the entire porous sample. This parameter accounts for the fact that the air inside the porous medium can be considered as volume added to the confined volume behind the porous medium.

(iv) The porous sample properties, i.e. porosity, tortuosity and Forchheimer coefficients, etc.

The specific implementation for the case of a blast wave impingement on a porous sample is used throughout the present study. This example is exploited in order to highlight the parameters affecting the pressure buildup at the shock tube end wall.

1.3. *Numerical modelling of shock wave interaction with a porous medium*

Earlier attempts to describe the fluid–porous interaction were based on a single-phase approach, which was based on a simplified averaged mixture theory. Such attempts were described, for example, by Gibson & Ashby (1988), Ben-Dor *et al.* (1994) and Mazor *et al.* (1994).

Another, more accurate, approach is the two-phase approach, which was first introduced by Biot (1941). In this approach, the microscopic phase balance equations are written for a representative elementary volume, REV, containing the gaseous and solid phases. Sorek *et al.* (1992) incorporated the Forchheimer term into the model of Bachmat & Bear (1986). It was not until Li, Levy & Ben-Dor (1995), Levy *et al.* (1996, 1998, 1999) and Levi-Hevroni *et al.* (2002, 2006) incorporated a more accurate presentation of the energy and the momentum transfer inside the porous medium that the model was capable of properly predicting the shock wave propagation inside a rigid porous sample. The aforementioned studies showed that in order to actually solve the system of governing equations, one has to determine the values of the parameters, namely the tortuosity, T^*, and the Forchheimer coefficient, F.

1.4. *Analytical modelling*

Ram & Sadot (2013) developed an empirical model (referred to as the RS model) which accounts for the physical parameters affecting the pressure buildup profile at the shock tube end wall. The model was described as a solution to the following first-order differential equation:

$$\frac{\mathrm{d}P(t)}{\mathrm{d}t} = \alpha(\mathrm{SOD} + L_{eff})^{-\gamma}(P_{in}(t) - P(t)), \tag{1.1}$$

where $P(t)$ is the pressure acting on the end wall, $P_{in}(t)$ is the input (enforcing) pressure profile that is imposed on the front face of the porous sample, α is a coefficient that lumps the material properties of the porous medium together, L_{eff} is the effective length of the porous sample (i.e. the sample length multiplied by its porosity) and γ is the specific heat capacity ratio of the air.

The model assumptions are that the porous sample significantly attenuates the shock wave transmitted through it and that the pressure buildup is achieved through an isentropic process. Furthermore, it was shown that a single shock tube experiment is sufficient to determine the value of α for a given porous sample. It should be recalled that α lumps the material properties of the porous medium together. As a

result, the pressure buildup profile could be predicted for a given incident shock wave and standoff distance. Ram & Sadot (2013) also showed that this model could be used to predict the pressure buildup using a variety of porous-like barriers such as a series of grids or perforated plates. While the RS model predicts very well the pressure buildup as a result of the impingement of constant-velocity shock waves (step jump) on the front face of porous samples, its validity is yet to be checked against other imposed pressure profiles such as the one that results from the impingement of blast waves (close to exponentially decaying).

The focus of the present study is to better understand the overall time-dependent pressure profile developing on the end wall, i.e. the target wall, when a layer made of porous medium is placed at a distance from the target wall, thus creating an air gap, by analysing the measured pressure signal modulation in the frequency domain. Furthermore, both the numerical model and the RS model are employed in order to further elaborate the physical mechanisms affecting the pressure profile at the end wall. Previously reported results had focused on the impingement of a shock wave generating a 'step function' in the pressure imposed on the front face of the porous sample. However, in this context, it is important to examine the more complex and more realistic case in which the pressure profile that is imposed on the front face of the porous sample changes in time after the instantaneous pressure jump that is imposed by the impingement of a blast wave.

1.4.1. *Experimentally determining* α

Figure 2(*a*) depicts four experiments in which a shock wave having an average Mach number of 1.567 impinges a sample made of a porous medium, generating an instantaneous step function pressure load, P_{step} (5.5 atm in this case). The recording at the end wall exhibits a minor sharp rise due to the transmitted shock wave. This small instantaneous jump is then followed by a gradual pressure increase which ceases when the pressure in the confined volume behind the porous medium reaches P_{step}. Figure 2(*a*) also depicts the dependence on the standoff distance; increasing the standoff distance prolongs the pressure buildup duration.

The four pressure records exhibit similar exponential behaviour, each with its unique time constant. Figure 2(*b*) shows a replot of the results shown in 2(*a*) in scaled time and normalized pressure according to the following definitions (Ram & Sadot 2013):

$$\tau = \frac{t}{(\mathrm{SOD} + L_{eff})^{\gamma}}, \tag{1.2}$$

$$P^{*} = \frac{P(\tau)}{P_{step}}, \tag{1.3}$$

where τ is a scaled time and P^{*} is the pressure load normalized by the pressure step function height, P_{step}.

This presentation eliminates the geometrical and initial conditions in the experiments. The scaled results are fitted to an exponential function (1.4), which is the solution of the analytical model (1.1) for a step function in $P_{in}(t)$,

$$P^{*} = 1 - \mathrm{e}^{-\alpha\tau}. \tag{1.4}$$

In (1.4), α is the only free parameter. Following this methodology, one can find α for various porous media. As stated above, α is a lumped parameter that effectively encapsulates the material properties affecting the flow through the porous medium.

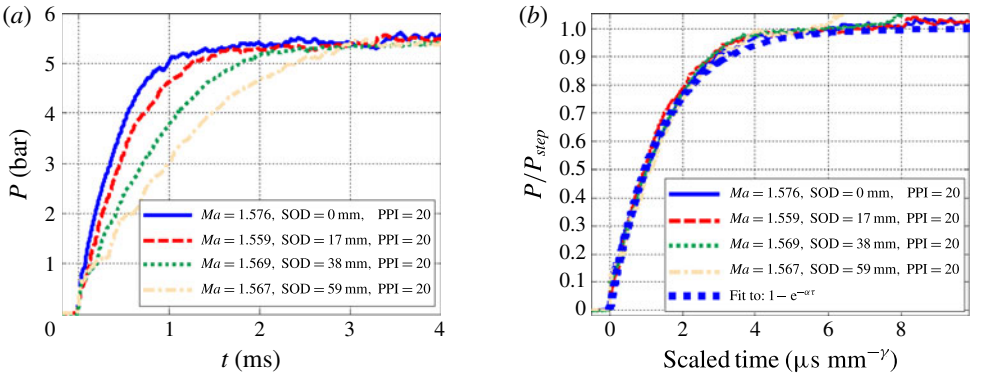

FIGURE 2. (Colour online) (*a*) End wall pressure histories recorded in a set of four experiments with different stand of distance (SOD) and the same number of pores per inch (PPI) and Mach number. (*b*) The same pressure histories presented in a scaled manner, and a fit to an exponential function.

Consequently, α depicts the effect of the porous medium properties on the pressure buildup duration. While this procedure is demonstrated here using four different experiments, it should be noted that just one is sufficient to replot the result in a scaled manner to find α by fitting the results to (1.4).

2. Experimental facilities

2.1. *Experimental apparatus*

The experimental investigation was conducted in the shock tube laboratory of the Protective Technologies R&D Center of the Ben-Gurion University of the Negev (BGU-PTR&DC). A vertical 4.5 m long shock tube with an internal cross-section of 80 mm × 80 mm was used. The shock tube was fitted with a short driver section, 0.1 m long. The driven and driver sections of the shock tube were separated by a fast opening valve. After pressurization of the driver section, the fast opening valve was activated using a remotely controlled servo motor. The generated blast waves interacted with the porous samples placed in the test section of the shock tube. The pressure histories (profiles) of the flow within the shock tube were recorded using four Endevco piezo-resistive pressure transducers, PT_i (model 8510B-500), and an electric Endevco amplifier (model 136). The pressure signals were converted to electric signals and monitored by a digital oscilloscope (LeCroy LT344 WaveSurfer). A schematic drawing of the experimental apparatus set-up and the data acquisition system is shown in figure 3. The shock wave and the data acquisition system were synchronized using an external in-house designed trigger box. The operation of the entire system was computer controlled through a LabView application. The control system was based on NI PCI-6602 and PCI-6035E I/O cards. The desired pressure in the driver section was set before the experiment and then controllably filled without intervention. The fast opening valve and the driver pressure automated control provided repeatability within a standard deviation of 0.3 % in the incident shock wave Mach number. The same shock tube system was also fitted with a 2.5 m long driver section. The driver and driven sections in this case were separated using a thin Mylar diaphragm. After pressurizing the driver section, the Mylar diaphragm was ruptured by means of a striking pin. The repeatability in the incident Mach number for this mode of operation was measured to be within 2 %.

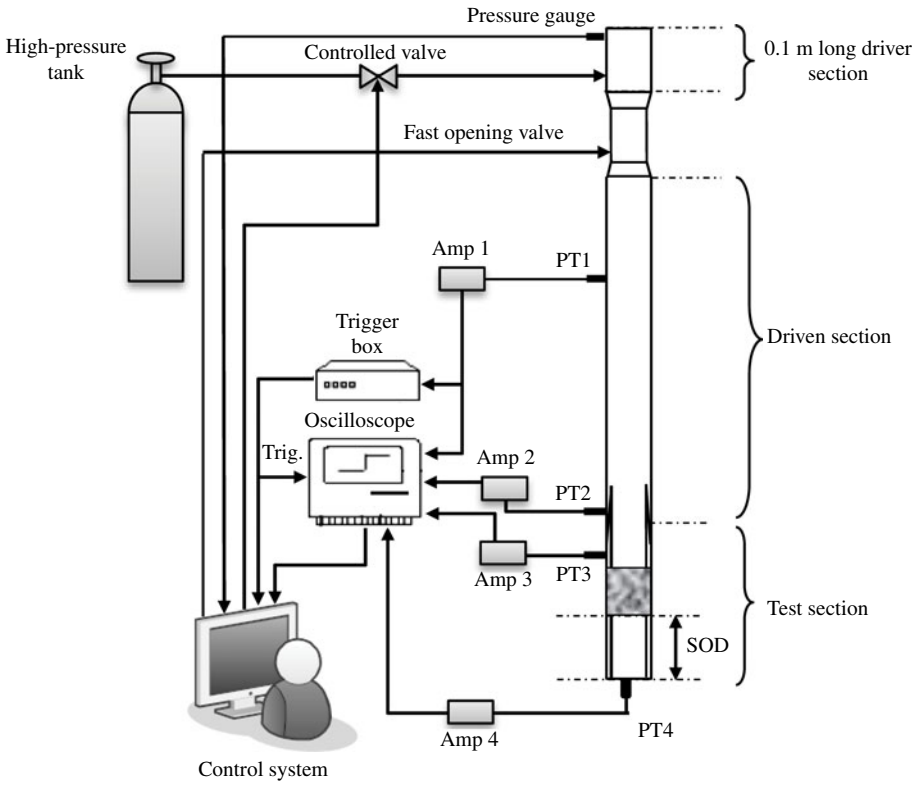

FIGURE 3. A schematic illustration of the experimental apparatus set-up and the data acquisition system.

2.2. *Short driver shock tube*

In order to generate a pressure pulse similar to that of a blast wave, the abovementioned vertical shock tube was fitted with a short driver section. In the past, the same shock tube facility was fitted with a long driver in order to generate a step function loading, which is more typical for conventional shock tubes. The results from this earlier study were used to formulate the RS model (Ram & Sadot 2013). Some of these results are also used in the present study to demonstrate some of the new points that are raised in the discussion section. Further information on this technique of generating blast-like pressure profiles can be found in Britan *et al.* (1993).

2.3. *The porous samples*

The rigid porous samples, SEDEX ceramic foam filters made of silicon carbide (SiC), were manufactured by Foseco and had three pore densities, 10, 20 and 30 pores per inch (PPI). The shape of the unit cell was pentagonal-dodecahedron. All of the samples were cut by the manufacturer to dimensions of 75 mm $\times$ 75 mm $\times$ 21 mm. In each of the experiments that are presented subsequently, three porous sample layers were stacked to form a 63 mm wide porous sample. The air volume fraction, i.e. porosity, of all the samples was measured to be $86\,\% \pm 5\,\%$.

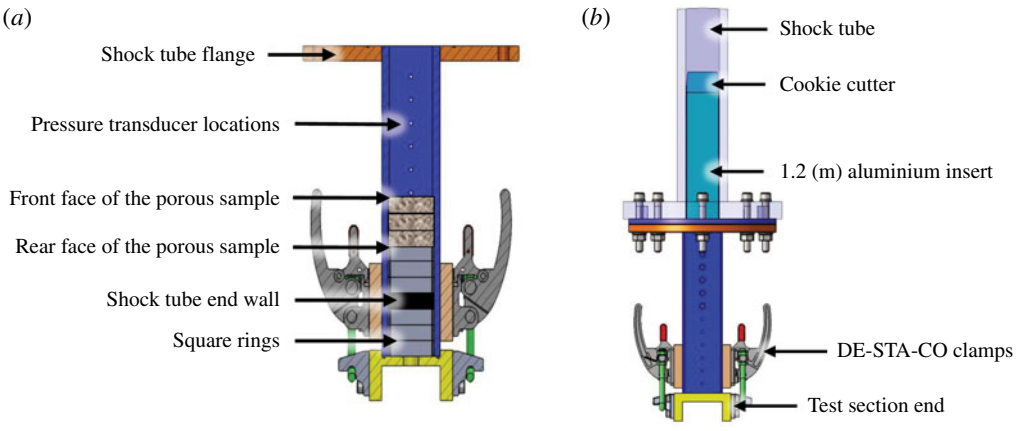

FIGURE 4. (Colour online) (*a*) The designed test section in which the porous samples were fixed. In this design, the location of the front face of the porous sample remained fixed while the end wall of the shock tube could be moved to facilitate different standoff distances. (*b*) A 1.2 m aluminium 'cookie cutter' was inserted into the shock tube to negotiate the cross-section area change.

2.4. *The test section*

In order to fix different porous samples in the shock tube test section, a special test section was custom designed and constructed (figure 4*a*). The test section design fulfilled two functions. It narrowed the cross-section of the shock tube (80 mm × 80 mm) to fit the dimensions of the porous sample (75 mm × 75 mm) and it enabled the porous samples to be held at different standoff distances, SOD, from the end wall of the shock tube. The cross-section of the shock tube was narrowed by placing a 'cookie cutter' facing the flow direction ending 1.2 m upstream of the front face of the porous sample (figure 4*b*). Square rings machined from aluminium were inserted as spacers between the porous samples and the end wall. Each square ring enabled the standoff distance to be incremented by 21 mm. The porous samples blocked the entire cross-section of the test section. The front face of the porous sample was at the same location in all of the experiments. The end wall of the shock tube could be moved to different locations in order to facilitate changes in the standoff distance.

3. Experimental results

Figure 5(*a–f*) represents six different sets of experiments, each performed with a different configuration. These experiments are presented in a way that highlights the effects of the properties of the porous sample and the standoff distance on the pressure profile at the end wall. Figure 5(*a–c*) represents a set of experiments that were conducted with three different porous samples, i.e. different PPI values, and a fixed standoff distance. Figure 5(*d–f*) represents a set of experiments that were conducted with various standoff distances and the same porous sample, i.e. the same PPI value. The standoff distance was varied by changing the position of the end wall in the range 0–80 mm. The pressure history as measured without a porous sample placed is added to each of the data sets presented in figure 5. This pressure profile is a reference for studying the effects of the porous medium on the pressure

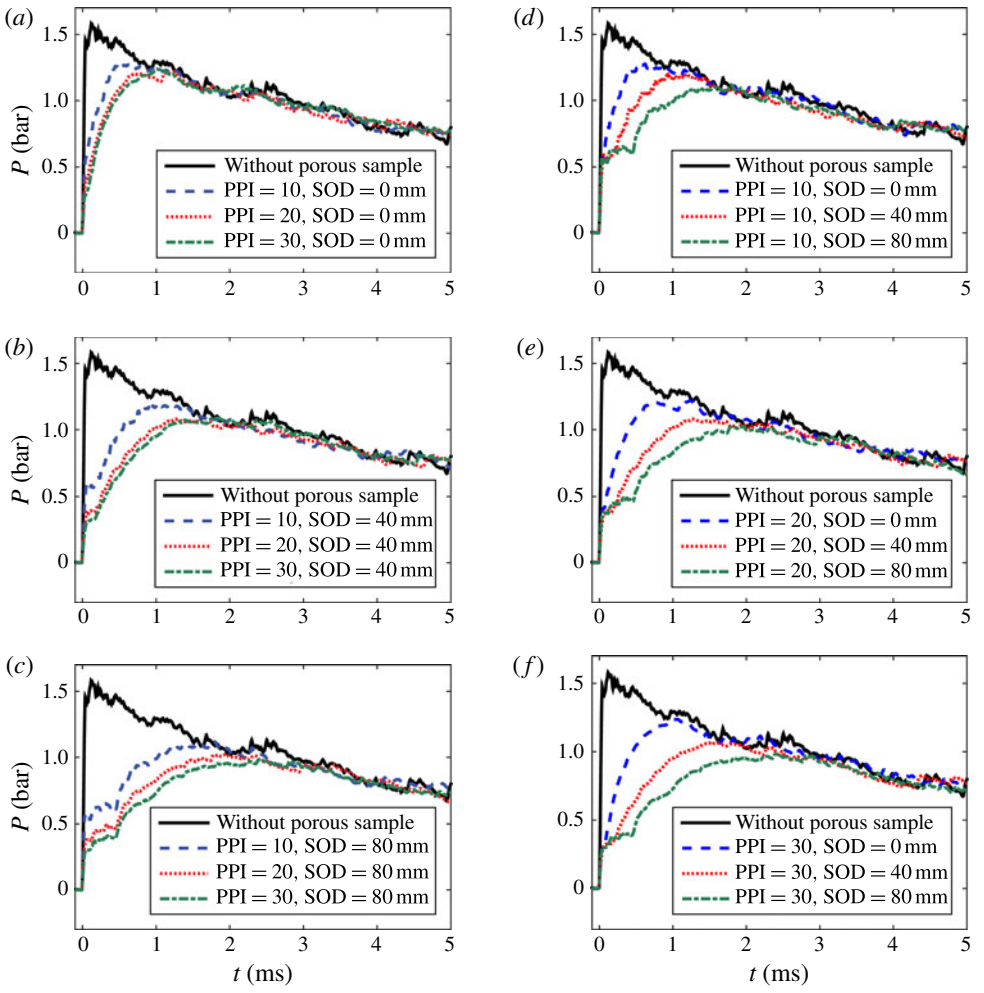

FIGURE 5. (Colour online) Experimental results highlighting the influence of the porous sample on the peak overpressure at the end wall: (*a–c*) the influence of the PPI of the sample; (*d–f*) the influence of the standoff distance. All of the experiments presented were performed with 10 bar driver pressure.

buildup. The first set of experiments reveals that as the PPI value of the porous sample increases, the peak overpressure decreases. The second set of experiments reveals that increasing the standoff distance results in a greater reduction of the peak overpressure.

4. Discussion

4.1. *Mechanical system analysis*

In order to better understand the mechanisms affecting the pressure profile that is developed on the shock tube end wall, we chose to examine the porous medium and the volume trapped behind it in the air gap as a single mechanical system. This mechanical system is schematically illustrated in figure 6. By considering the problem in this manner, one can refer to the system as a lumped element. In this system, the

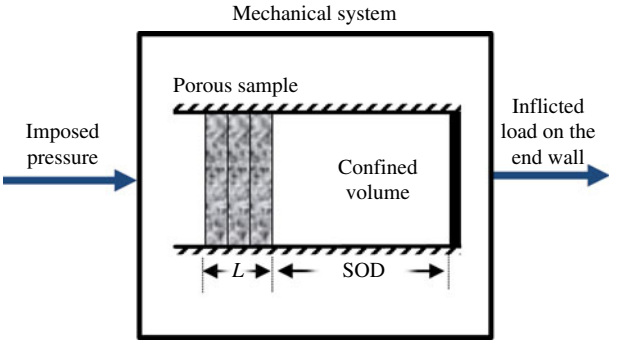

FIGURE 6. (Colour online) A schematic illustration of the mechanical system that transfers the input pressure waveform to an output pressure waveform. The system parameters are the length of the porous sample, L, the standoff distance, SOD, and the porous material properties.

input is the pressure profile imposed on the front face of the porous sample, whereas the output is the pressure profile that is developed on the shock tube end wall. If the transformation between the input and the output of the mechanical system can be characterized, a better understanding of the transformation of the pressure profile through the porous sample and the confined volume can be achieved.

4.1.1. *The modal response of the system*

The analysis of the mechanical system shown in figure 6 provides tools for broadening the discussion about the mechanisms affecting the pressure profile transformation through the porous sample. To characterize the behaviour of the system, one must first discuss the system response to a step function (such as that provided by a planar shock wave moving with a constant velocity). The system initially lies in a state of equilibrium when the input signal is zero. Imposing a step function (by a shock wave) instantly changes the input from its value just before $t = 0$ by a given amount. At this stage, the input level is kept constant at the new value. This leads to a transient response known as the step response of the system (Figliola & Beasley 2011).

The shock wave that is formed in a conventional shock tube generates an instantaneous step jump in the pressure, i.e. a step function, which is as ideal as one might expect to have when trying to study the transient response of the system. The step function imposed by the shock wave is characterized by some amplitudes in all of the frequencies. Comparison of the amplitude in each specific frequency of the system output with respect to the system input provides a new understanding of the mechanisms affecting the pressure profile transformation.

A typical response of the system, based on the Ram & Sadot (2013) differential description of the system, is presented in figure 7(*a*) for various configurations. Application of the suggested method revealed that in the frequency domain, the amplitudes associated with high frequencies are significantly attenuated. The system in fact acts as a low-pass filter on the time-dependent pressure input. Figure 7(*b*) shows the ideal step function (black line), the predicted pressure profiles (dashed coloured lines) acquired using a low-pass filter as obtained from (1.1) and the actual measured pressure profile at the system output imposed with a shock-wave-induced step function at the system input (solid coloured lines).

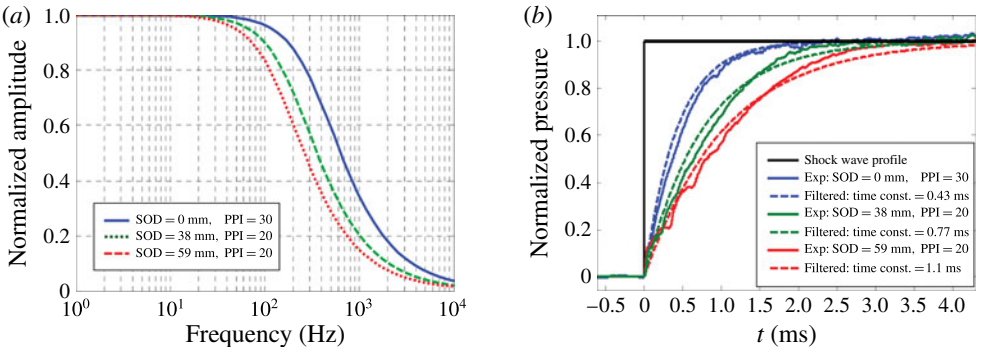

FIGURE 7. The modal response of the mechanical system comprising the porous sample and the confined volume (see figure 6). Three examples are shown which relate to different configurations of the porous sample, the PPI and the standoff distance, SOD. As the cutoff frequency decreases, the pressure rise becomes slower.

It should be noted that some differences are apparent, as they are caused by some shock waves passing through the porous sample and reverberating back and forth inside the confined volume. These shock waves are not accounted for when the low-pass filtering approach is used. Nevertheless, the model predictions are in good agreement with the experimental results.

Interpreting the system as a low-pass filter suggests that pressure pulses that are dominated by high frequencies at early stages (such as presented in this study) will be dramatically altered during these stages.

4.1.2. *Evaluation of the time constant of the system*

As demonstrated above, the main parameter affecting the pressure profile measured on the end wall of the shock tube is the time constant of the system. Based on the RS model, the time constant of the system can be calculated directly as $\alpha(L_{eff} + \mathrm{SOD})^{-\gamma}$, in which L_{eff}, SOD and γ are known for a specific experiment. However, the parameter α, which lumps the affecting properties of the porous medium together, is not well defined and requires further elaboration.

The methodology presented in § 1.4.1 should be followed to experimentally determine α. As shown, the experimental result from a single shock tube experiment should be replotted in a scaled form accounting for the influence of the standoff distance, sample length and the incident shock wave Mach number (Ram & Sadot 2013). An exponential function, which is a function of α, should be fitted to the experimental results. Once the value of α is determined for a given porous material, the output pressure at the rear face of the porous sample can be calculated for any given input pressure that is imposed on the front face of the same porous sample.

Since the number of samples used in this study is limited, the model and the numerical solution that were developed by Levy *et al.* (1996) were used to determine α for other porous materials. Levy *et al.*'s (1996) model was extensively validated, and it predicted very well the pressure output buildup in one-dimensional numerical simulations. The geometrical dimensions of the problem were reduced to the length of the porous sample, L, and the standoff distance, SOD. A comparison between experimental results for various configurations with a long driver section (i.e. constant-velocity planar shock waves) and their corresponding numerical simulations

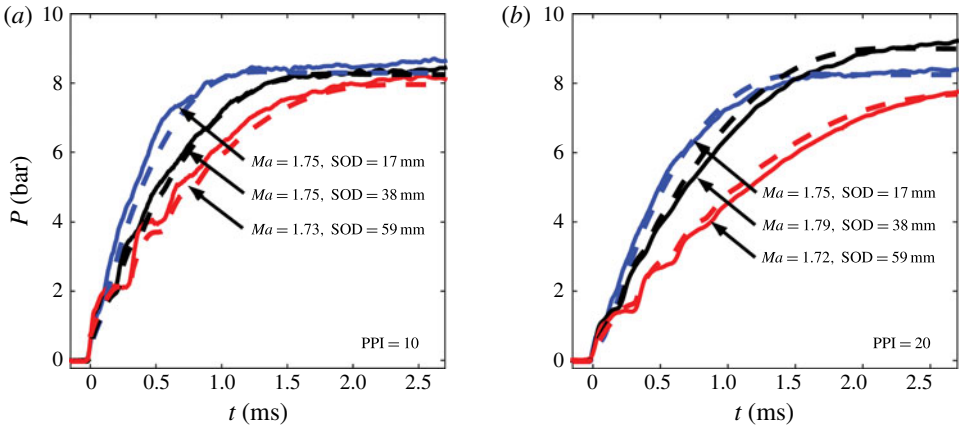

FIGURE 8. (Colour online) A comparison between the experimental results (solid lines) for a constant-velocity planar shock wave configuration and the corresponding numerical simulations (dashed lines), showing a very good agreement between the two.

is presented in figure 8. The experimental results for various samples with different values of the PPI and different initial conditions are compared with the numerical simulations. The comparison reveals a very good agreement between the experimental results and the numerical simulations.

Figure 9(*a*) shows the dependence of α on the affecting material properties, i.e. the Forchheimer and tortuosity coefficients, as was obtained numerically. All of the numerical simulations were conducted using a 40 mm standoff distance, a 60 mm long porous sample and an incident shock wave Mach number equal to 1.5. In order to determine α, the numerical results were scaled according to the RS model and fitted with an exponential function.

The numerical results that show the dependence of α on the two parameters (Forchheimer coefficient and tortuosity) indicate that among the two, the resistance to the flow, i.e. the Forchheimer coefficient, is the more dominant one. Figures 9(*b*) and 9(*c*) strengthen this finding by showing that α depends on the Forchheimer coefficient in an exponentially decaying manner and on the tortuosity in a linear increasing manner.

4.2. *Predicting the pressure profile on the end wall*

The mechanical system approach presented above can be used to predict the pressure profile that will develop on the shock tube end wall. The enforcing (input) pressure profile is the pressure profile measured without a porous sample (i.e. $P_{in}(t)$ in (1.1)). Figure 10 shows the predicted pressure profiles that were obtained by means of (1.1). The smooth rise of the resulting pressure profiles indicates that the changes associated with the high frequencies were filtered out. As can be seen, the model predicts quite well the peak overpressures and the buildup duration times. However, since the model does not account for the shock wave transmitted through the porous sample, a difference is seen for configurations with long standoff distances. This is due to the fact that the transmitted shock wave travels a long way before it reaches the shock tube end wall and upon its head-on reflection it causes a sharp pressure jump. This sharp pressure jump is not accounted for in the RS model. Once the

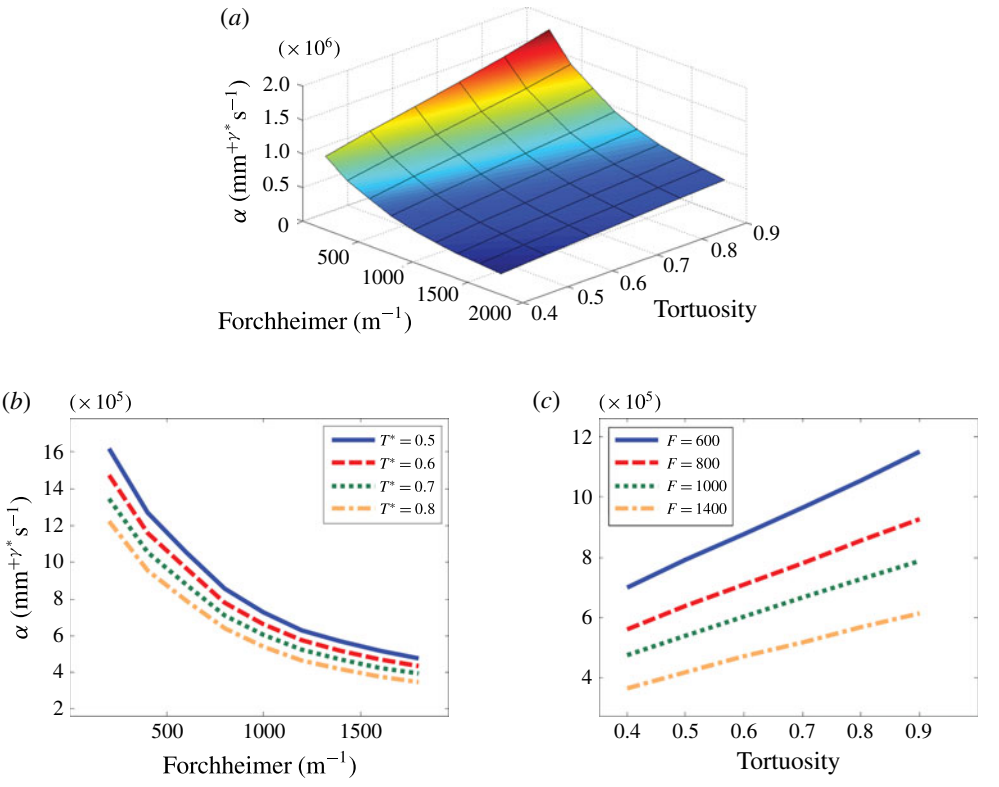

FIGURE 9. (Colour online) (*a*) The dependence of α on the Forchheimer and tortuosity coefficients as obtained numerically. (*b*) The dependence of α on the Forchheimer coefficient has an exponentially decaying form. (*c*) The dependence of α on the tortuosity has a linear increasing manner.

transmitted shock wave is reflected, the pressure rise becomes moderate and closer to that achieved through an isentropic process. This stage of the pressure buildup is well described by the RS model.

It is important to note that due to differences in the flow into the porous sample after the head-on reflection of the incident shock wave and due to the changes in the strength of the reflected wave, the conditions at the front face of the porous sample are not the same for the different experiments. Nevertheless, since the wave transmitted through the porous sample is weak and the lumped parameter, α, accounts for this effect, the input pressure profile of the model should be taken as the pressure profile developed on a rigid wall.

4.3. *Physical mechanism for the pressure buildup duration*

The results presented above indicate that the assumption of a macroscopic approach provides the means to simply explain the physical mechanism without solving the specific microscopic flow–structure interaction. This methodology might be conceived as an oversimplification of the problem; however, one should note that while the problem of shock interaction with rigid porous barriers had been studied for many years, the understanding of the physical behaviour of the transient flow through the porous medium and the shock–structure interaction is still quite limited. This is

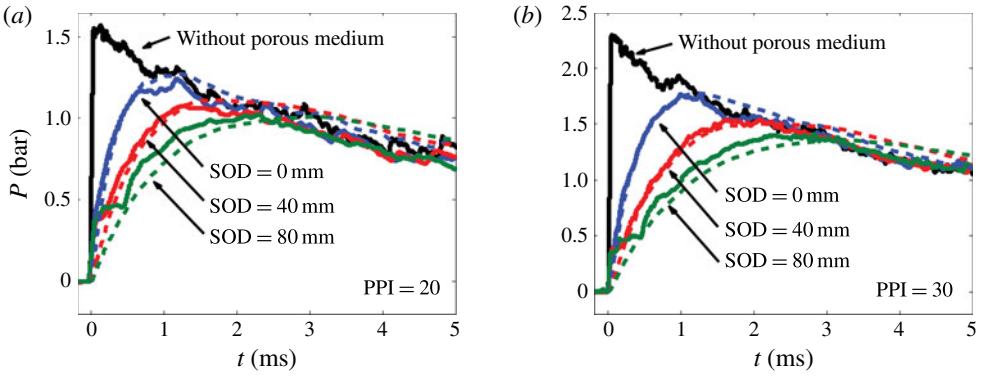

FIGURE 10. (Colour online) Predicted pressure profiles obtained using (1.1) for experiments performed with (*a*) 10 bar and (*b*) 15 bar in the driver section. In this figure, various experiments (coloured solid lines) are compared with the model predictions (dashed lines). In the model, the reference profile (black solid line) was used as the input pressure and α was taken for a 20 PPI and 30 PPI sample from Ram & Sadot (2013).

even more pronounced when dealing with scenarios where the properties behind the incident shock wave are not constant (i.e. not generating a step function). Strictly speaking, the scenario presented in this study was chosen specifically since a rather good numerical solution exists (see § 4.1.2), but this is not the general case in such problems. There are various problems in the open literature dealing with shock–structure interaction to which the methodology presented in this paper applies. Figure 11 presents two such examples. Figure 11(*a*) shows that when a shock wave impinges on a thin layer of granular medium, a similar pressure profile to that found in the present study is recorded. For this scenario, taken from a series of studies focused on shock-wave–granular-medium interaction, one can find only approximate solutions, which are based on oversimplified models (see, for example, Britan *et al.* 2001). Furthermore, examination of a scenario where a shock wave impinges a barrier comprising two perforated plates spaced 45 mm away from each other and placed with a 140 mm standoff distance to the end wall reveals once again a very similar behaviour (Seeraj & Skews 2009). A detailed solution of these problems requires one to obtain numerous parameters such as the viscous resistance to the flow, the tortuosity, the volume fraction of the air, the solid stiffness, etc. Some of these can be easily measured and some (e.g. the viscous resistance to the flow and the tortuosity) are quite elusive and require elaborate experimental testing. Furthermore, the modelling and solution strategy is unique to each barrier type.

The methodology of examining the whole problem in a macroscopic manner, taking the porous medium and the air confined between the porous medium and the end wall, is valid for these cases as well. The results presented and the corresponding discussion yield a new understanding of the physics involved in these problems. In all of these problems, one finds an inhibitor to the flow (i.e. porous medium, granular medium, perforated plates, etc.) and a reservoir of air. These two elements are combined to determine the pressure buildup on the end wall.

In this regard, we can now stipulate that the model presented in (1.1) not only describes the results presented in this paper but can be modified to study more elaborate problems as well. The inhibition to the flow facilitated by the porous barrier will lump into α given a specific standoff distance and a specific imposed pressure profile.

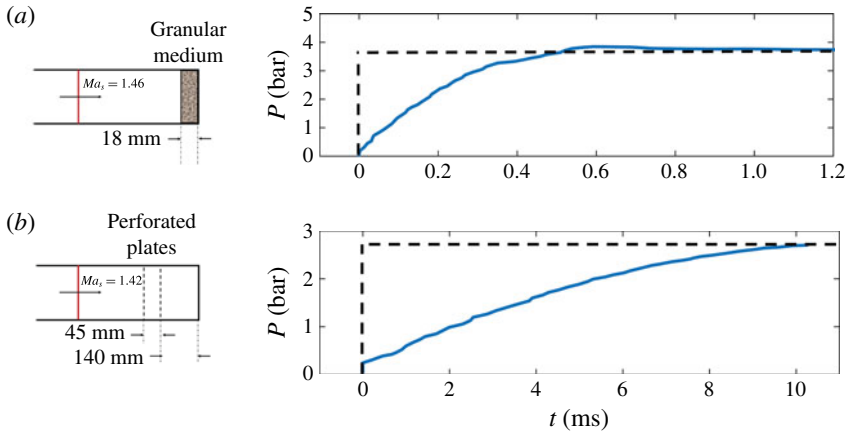

FIGURE 11. (Colour online) (*a*) The pressure profile recorded on the end wall of a shock tube behind an 18 mm thick layer of granular medium comprising 0.5 mm diameter spheres (resampled from Britan *et al.* 2001, figure 9). (*b*) The pressure profile recorded on the end wall of a shock tube behind two perforated plates spaced 45 mm from each other and with a standoff distance of 140 mm from the end wall (resampled from Seeraj & Skews 2008, figure 18).

5. Conclusions

The effects of the parameters governing the pressure transformation through a porous sample impinged by a pressure pulse were demonstrated. It was found that the influence of the standoff distance between the rear face of the porous sample and the end wall of the shock tube is very significant. It was also found that the pressure buildup duration, which is governed by the standoff distance and the geometrical material properties, i.e. the Forchheimer and tortuosity coefficients, effectively reduces the impulse and hence determines the protection provided by the porous barrier. The chosen mechanical system perspective enabled us to better understand the basic mechanisms affecting the pressure profile transformation while passing through the porous sample and the air gap between the rear face of the porous sample and the shock tube end wall. The modal response of the system revealed that when an arbitrary pressure pulse was imposed on the front face of the porous sample the amplitudes associated with the high frequencies were attenuated. It was inferred from the results that the confined volume behind the porous sample acted as an absorbing buffer, which dispersed the changes in the pressure. As the confined volume increased, the mass of the air inside it also increased. As a result, the time constant of the pressure change due to the imposed changing input conditions increased as well. This in turn attenuated the amplitude in the high frequencies. This understanding, which sprang directly from the previously presented RS model (Ram & Sadot 2013), sheds more light and understanding on the effects of the porous medium.

It was also shown that once the RS model was calibrated correctly to account for the porous sample properties by determining the time constant of the system, i.e. α, it provided the means to predict the pressure buildup profile on the shock tube end wall. Although this was illustrated for two types of pressure profiles that were generated in the shock tube (the pressure profiles behind a constant-velocity moving shock wave

and an attenuating shock wave, i.e. a blast wave), it could be done for any given time-dependent pressure profile.

Acknowledgements

This work was supported in part by Plasan Sasa Ltd and the Israel Science Foundation (ISF) under grant no 139/10. O.R. is supported by the Adams Scholarship Program of the Israeli academy of science. The authors thank Professor G. Ben-Dor, Professor A. Levy and Ms M. Geva for their constructive suggestions and support.

REFERENCES

ANDREOPOULOS, Y., XANTHOS, S. & SUBRAMANIAM, K. 2007 Moving shocks through metallic grids: their interaction and potential for blast wave mitigation. *Shock Waves* **16**, 455–466.

BACHMAT, Y. & BEAR, J. 1986 Macroscopic modelling of transport phenomena in porous media. 1: the continuum approach. *Transp. Porous Med.* **1**, 213–240.

BALL, G. J. & EAST, R. A. 1999 Shock and blast attenuation by aqueous foam barriers: influences of barrier geometry. *Shock Waves* **9**, 37–47.

BEN-DOR, G., MAZOR, G., CEDERBAUM, G. & IGRA, O. 1996*a* Well tailored compressive stress–strain relations for elastomeric foams. *J. Mater. Sci.* **31**, 1107–1113.

BEN-DOR, G., MAZOR, G., CEDERBAUM, G & IGRA, O. 1996*b* Stress–strain relations for elastomeric foams in uni-, bi- and tri-axial compression modes. *Arch. Appl. Mech.* **66**, 409–418.

BEN-DOR, G., MAZOR, G., CEDERBAUM, G., IGRA, O. & SOREK, S. 1992 The enhancement of shock wave loads by means of porous media. (ed. K. Takayama), Shock Waves SE - 39, pp. 279–282. Springer.

BEN-DOR, G., MAZOR, G., IGRA, O., SOREK, S. & ONODERA, H. 1994 Shock wave interaction with cellular materials. *Shock Waves* **3**, 167–179.

BENSELAMA, A. M., WILLIAM-LOUIS, M. J. P., MONNOYER, F. & PROUST, C. 2010 A numerical study of the evolution of the blast wave shape in tunnels. *J. Hazard. Mater.* **181**, 609–616.

VAN DEN BERG, A. C. & WEERHEIJM, J. 2006 Blast phenomena in urban tunnel systems. *J. Loss Prev. Process. Ind.* **19**, 598–603.

BERGER, S., SADOT, O. & BEN-DOR, G. 2010 Experimental investigation on the shock-wave load attenuation by geometrical means. *Shock Waves* **20**, 29–40.

BERGER, S., SADOT, O. & BEN-DOR, G. 2012 Numerical investigation of shock-wave load attenuation by barriers. In *28th International Symposium on Shock Waves* (ed. K. Kontis), pp. 111–116. Springer.

BIOT, M. A. 1941 General theory of three-dimensional consolidation. *J. Appl. Phys.* **12**, 155–164.

BRITAN, A., BEN-DOR, G., IGRA, O. & SHAPIRO, H. 2001 Shock wave attenuation by granular filters. *Intl J. Multiphase Flow* **27**, 617–634.

BRITAN, A., IGRA, O., BEN-DOR, G. & SHAPIRO, H. 2006 Shock wave attenuation by grids and orifice plates. *Shock Waves* **16**, 1–15.

BRITAN, A., LIVERTS, M., SHAPIRO, H. & BEN-DOR, G. 2012 Blast wave mitigation by a particulate foam barrier. *Transp. Porous Med.* **93**, 283–292.

BRITAN, A., SHAPIRO, H., LIVERTS, M., BEN-DOR, G., CHINNAYYA, A. & HADJADJ, A. 2013 Macro-mechanical modelling of blast wave mitigation in foams. Part I: review of available experiments and models. *Shock Waves* **23** (1), 5–23.

BRITAN, A. B., VASILEV, E. I., ZINOVIK, I. N. & KAMYNIN, I. Y. 1993 Reflection of a blast-profile shock wave from the end wall of a shock tube. *Fluid Dyn.* **27** (3), 412–417.

FIGLIOLA, R. S. & BEASLEY, D. E. 2011 *Theory and Design for Mechanical Measurements*. Wiley.

GIBSON, L. & ASHBY, H. 1988 *Cellular Solids: Structure and Properties*. Pergamon.

IGRA, O., FALCOVITZ, J., HOUAS, L. & JOURDAN, G. 2013 Review of methods to attenuate shock/blast waves. *Prog. Aerosp. Sci.* **58**, 1–35.

KAZEMI-KAMYAB, V., SUBRAMANIAM, K. & ANDREOPOULOS, Y. 2011 Stress transmission in porous materials impacted by shock waves. *J. Appl. Phys.* **109** (1), 013523.

KITAGAWA, K., YASUHARA, M. & TAKAYAMA, K. 2006 Attenuation of shock waves propagating in polyurethane foams. *Shock Waves* **15**, 437–445.

LANGDON, G. S., NURICK, G. N. & DU PLESSIS, N. J. 2011 The influence of separation distance on the performance of perforated plates as a blast wave shielding technique. *Engng Struct.* **33**, 3537–3545.

LARSEN, M. E. 1992 Aqueous foam mitigation of confined blasts. *Intl J. Mech. Sci.* **34**, 409–418.

LEVI-HEVRONI, D., LEVY, A., BEN-DOR, G. & SOREK, S. 2002 Numerical investigation of the propagation of planar shock waves in saturated flexible porous materials: development of the computer code and comparison with experimental results. *J. Fluid Mech.* **462**, 285–306.

LEVI-HEVRONI, D., LEVY, A., BEN-DOR, G. & SOREK, S. 2006 The interaction of planar shock waves with multiphase saturated flexible porous materials – a numerical investigation. *J. Fluid Mech.* **563**, 159–188.

LEVY, A., BEN-DOR, G., SKEWS, B. W. & SOREK, S. 1993 Head-on collision of normal shock waves with rigid porous materials. *Exp. Fluids* **15**, 183–190.

LEVY, A., BEN-DOR, G. & SOREK, S. 1996 Numerical investigation of the propagation of shock waves in rigid porous materials: development of the computer code and comparison with experimental results. *J. Fluid Mech.* **324**, 163–179.

LEVY, A., BEN-DOR, G. & SOREK, S. 1998 Numerical investigation of the propagation of shock waves in rigid porous materials: flow field behavior and parametric study. *Shock Waves* **8**, 127–137.

LEVY, A., LEVI-HEVRONI, D., SOREK, S. & BEN-DOR, G. 1999 Derivation of Forchheimer terms and their verification by application to waves propagation in porous media. *Intl J. Multiphase Flow* **25**, 683–704.

LI, H., LEVY, A. & BEN-DOR, G. 1995 Head-on interaction of planar shock waves with ideal rigid open-cell porous materials. Analytical model. *Fluid Dyn. Res.* **16**, 203–215.

MAZOR, G., BEN-DOR, G., IGRA, O. & SOREK, S. 1994 Shock wave interaction with cellular materials. *Shock Waves* **3**, 159–165.

OHTOMO, F., OHTANI, K. & TAKAYAMA, K. 2005 Attenuation of shock waves propagating over arrayed baffle plates. *Shock Waves* **14**, 379–390.

OLIM, M., VAN DONGEN, M. E. H., KITAMURA, T. & TAKAYAMA, K. 1994 Numerical simulation of the propagation of shock waves in compressible open-cell porous foams. *Intl J. Multiphase Flow* **20**, 557–568.

ONODERA, H. 1998 Shape of a shock wave front diffracting on a perforated wall. *Exp. Fluids* **24**, 238–245.

PANCZAK, T. D., KRIER, H. & BUTLER, P. B. 1987 Shock propagation and blast attenuation through aqueous foams. *J. Hazard. Mater.* **14**, 321–336.

RAM, O. & SADOT, O. 2013 A simple constitutive model for predicting the pressure histories developed behind rigid porous media impinged by shock waves. *J. Fluid Mech.* **718**, 507–523.

SEERAJ, S. & SKEWS, B. W. 2009 Dual-element directional shock wave attenuators. *Exp. Therm. Fluid Sci.* **33**, 503–516.

SEITZ, M. W. & SKEWS, B. W. 2006 Effect of compressible foam properties on pressure amplification during shock wave impact. *Shock Waves* **15**, 177–197.

SILVESTRINI, M., GENOVA, B. & LEON TRUJILLO, F. J. 2009 Energy concentration factor. A simple concept for the prediction of blast propagation in partially confined geometries. *J. Loss Prev. Process. Ind.* **22**, 449–454.

SKEWS, B. W. 1991 The reflected pressure field in the interaction of weak shock waves with a compressible foam. *Shock Waves* **1**, 205–211.

SKEWS, B. W., ATKINS, M. D. & SEITZ, M. W. 1992 Gas dynamic and physical behaviour of compressible porous foams struck by a weak shock wave. In *Shock Waves* (ed. K. Takayama), pp. 511–516. Springer.

SOREK, S., BEAR, J., BEN-DOR, G. & MAZOR, G. 1992 Shock waves in saturated thermoelastic porous media. *Transp. Porous Med.* **9**, 3–13.